minerals

MDPI

Article

On the Nature of Hydrophobic Organic Compound Adsorption to Smectite Minerals Using the Example of Hexachlorobenzene-Montmorillonite Interactions

Peter Grančič [1,*], Leonard Böhm [2], Martin H. Gerzabek [1] and Daniel Tunega [1,*]

[1] Institute of Soil Research, Department of Forest and Soil Sciences, University of Natural Resources and Life Sciences Vienna, Peter-Jordan-Straße 82, 1190 Vienna, Austria; martin.gerzabek@boku.ac.at
[2] Institute of Soil Science and Soil Conservation, Research Centre for BioSystems, Land Use and Nutrition (iFZ), Justus Liebig University Giessen, Heinrich-Buff-Ring 26, 35392 Giessen, Germany; leonard.boehm@umwelt.uni-giessen.de
* Correspondence: peter.grancic@cantab.net (P.G.); daniel.tunega@boku.ac.at (D.T.); Tel.: +43-1-47654-91137 (P.G.); +43-1-47654-91148 (D.T.)

Abstract: The fate of chemical pollutants in the environment is determined by various factors including the type and strength of their interactions with reactive surfaces in soils and sediments. In the present work the interactions of hexachlorobenzene (HCB) with the surface of a common clay mineral belonging to the smectite group montmorillonite (MNT) is studied by means of the density functional theory method. The MNT net surface charge, induced by isomorphic substitutions, is systematically varied and compensated by Ca^{2+} cations. Based on the calculated electron densities, conclusions are drawn revealing the nature of their mutual interactions, the related stability of such surface complexes as well as possible molecular arrangements. It becomes apparent that the dominant contribution to the stability of HCB-MNT complexes arises from the cation-π interactions between the HCB molecule and the nearest compensating Ca^{2+} cation and thus besides the MNT net surface charge the type and size of the compensating cations are expected to play a crucial role in understanding the HCB adsorption on MNT. This systematic study aims to contribute to a better mechanistic understanding of the interactions between hydrophobic organic compounds and reactive mineral surfaces.

Keywords: hydrophobic organic compounds; hexachlorobenzene; adsorption; smectite; montmorillonite; density functional theory

Citation: Grančič, P.; Böhm, L.; Gerzabek, M.H.; Tunega, D. On the Nature of Hydrophobic Organic Compound Adsorption to Smectite Minerals Using the Example of Hexachlorobenzene-Montmorillonite Interactions. *Minerals* **2023**, *13*, 280. https://doi.org/10.3390/min13020280

Academic Editor: Runliang Zhu

Received: 30 December 2022
Revised: 2 February 2023
Accepted: 14 February 2023
Published: 16 February 2023

1. Introduction

The development of modern societies is inevitably linked to the use of synthetic chemicals, many of which can cause undesired and often unpredicted impacts to the environment and biota. Particularly problematic are hydrophobic organic chemicals (HOCs) belonging to the class of persistent organic pollutants. The chlorinated aromatic hydrocarbon hexachlorobenzene (HCB) has been extensively used in agriculture as fungicide to control wheat bunt and smut fungi on other grains, as chemical intermediate in dye manufacture or additive for pyrotechnic compositions, synthetic rubber and polyvinyl chloride [1]. During its commercial production period (from 1930s until 1970s) a relatively large amount of HCB has been released into the environment. Its animal and possibly human carcinogenicity in combination with its environmental persistence pose a serious problem to the society [2].

Owing to its low solubility in aqueous environment and significant hydrophobic character [3], a considerable amount of HCB can be nowadays found in soils and sediments bound either to soil organic matter (SOM) or attached on mineral surfaces [1,4]. While the adsorption of HCB or other HOCs to SOM attracted significant attention [5–10], its interaction with mineral surfaces is still poorly understood. In our recent work the adsorption

of HCB to phyllosicate minerals is studied both, experimentally and computationally [11]. Mineral fractions quantitatively dominate the composition of soils and sediments, hence the fate and transport of HOCs are closely linked to their interactions with mineral surfaces.

Montmorillonite (MNT) is one of the most abundant 2:1 smectite-type layered phyllosilicates with a single layer composed of two silica tetrahedral sheets sandwiching a single alumina octahedral sheet. Isomorphic substitutions of Al or Si involving atoms of lower oxidation state naturally occur in either the tetrahedral and/or the octahedral sheet, causing a significant charge imbalance, and thus inducing a permanent negative net charge at the external surfaces. This excess negative charge is naturally balanced with inorganic cations, that are often hydrated and reside in the interlayer space [12–14]. The typical characteristics of MNT are structural expandability upon increasing hydration (swelling), high cation-exchange capacity (CEC, ranging between 60 and 100 mmol per 100 g of MNT), large surface area (typically about 80 m^2/g) and particularly fine particle size [15].

The application of computer modeling has proven to be a successful tool in explaining interactions of mineral surfaces with various hydrophobic moieties at the molecular level. For example, the formation of environmentally persistent free radicals as a result of an activation reaction of pentachlorophenol adsorbed on Fe^{3+}-modified MNT surface has been studied using density functional theory (DFT) [16]. Depending on the conformation, either non-bonded interactions between complementary partial charges or cation-π interactions play a crucial role in stabilizing the resulting complex. Similarly, the interactions of a set of polycyclic aromatic hydrocarbon molecules on MNT modified with transition metal cations was modeled by employing the DFT method [17]. In principle, the level of details provided by *ab initio* methods allows for the prediction of a variety of experimentally measurable quantities, such as dipole moments, vibrational modes and thermodynamic properties as in the case of the theoretical study of sulfur-containing aromatic hydrocarbons adsorbed on pyrophyllite [18]. The exchangeable cations are expected to play a significant role in the adsorption process of polyaromatic hydrocarbons on mineral surfaces [19–21].

The aim of the present article is to study HCB-MNT interactions by employing a geometry optimization machinery within the DFT framework *in vacuo* (not involving solvent effect) through the analysis of the resulting interaction energies, charge density and geometry characteristics of HCB-MNT complexes by systematically varying the MNT net surface charge.

2. Methodology

2.1. Structural Models

The initial geometry of the MNT unit cell was taken from Viani et al. [22]. Using a home-made script, first a slab composed of $4 \times 2 \times 1$ unit cells with the dimensions of $20.72 \times 17.96 \times 50$ $Å^3$ is constructed, exclusive of exchangeable cations. Next, isomorphic substitutions are introduced involving atoms of lower oxidation state in either the tetrahedral (e.g., Al^{III} replacing Si^{IV}) and/or the octahedral (e.g., Mg^{II} or Fe^{II} replacing Al^{III}) sheet by obeying the Löwenstein's substitution rule (i.e., the substitution sites cannot be adjacent to each other) [23], leading to a significant charge imbalance, and thus inducing a permanent negative charge at the external surfaces. Considering the size of the slab here, a single isomorphic substitution changes the MNT net surface charge by $-0.125\,|e|$. For each MNT net surface charge value q, several permutations of the isomorphic substitutions are created randomly. Further, the MNT net surface charge q is balanced by the addition of divalent calcium compensating cations (Ca^{2+}, CCC) distributed evenly with respect to both surfaces (in the case of odd number of isomorphic substitutions, the MNT net charge balance is achieved with the aid of a single monovalent Na^+ cation or F^- anion). Finally, a single HCB molecule is positioned in the vicinity of a selected CCC.

Due to the computational costs required here, it is impossible to sample the initial positions (in terms of translation and rotation with respect to arbitrary reference vector) of the planar and relatively rigid HCB molecule thoroughly. The initial positioning of the HCB molecule is therefore limited to the following three cases: (i) top-parallel, i.e., centered

above the CCC and parallel to the slab surface, (ii) tilted, i.e., positioned next to the CCC and rotated by 45° with respect to the slab surface and (iii) side-parallel, i.e., positioned aside of the CCC and parallel to the slab surface (cf. Figure 1). The geometry of these models is then optimized by the methodology described in the following section.

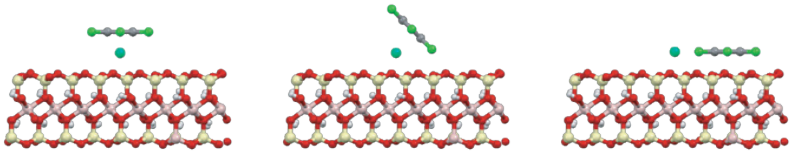

(a) (b) (c)

Figure 1. Initial configurations prior to geometry optimization, (**a**) top-parallel, (**b**) tilted and (**c**) side-parallel.

2.2. Computational Details

All electronic structure calculations were performed using the Vienna *ab initio* simulation package (VASP) [24–27]. To boost the geometry optimization procedure, the Gadget package was used [28]. The Kohn-Sham equations were solved variationally in a plane wave basis set with an energy cut-off of 400 eV. The generalized gradient approximation (GGA) [29] was used for the description of electron exchange-correlation terms using Perdew-Burke-Ernzerhof (PBE) functional [30]. Based on several benchmark studies [31–33] that compared the performance of various dispersion correction schemes in predicting non-bonding interactions, in our work we used D3 dispersion correction to the PBE functional [34] with the Becke-Johnson damping [35–37]. The cited benchmark works showed that the PBE-D3 method is able to predict nonbonding interactions such as cation-π or hydroxyl group-π with an acceptable accuracy. Electronic structure of the atoms was expressed by pseudo-potentials using the projector-augmented wave method [38,39]. A single Γ-point sampling was used for the integration over the Brillouin zone. The geometry optimisation was considered completed when the maximum force acting on a single atom was less than 0.01 eV $Å^{-1}$ for atomic positions and the electronic steps were considered converged if the difference in the energy was lower than 10^{-6} eV. For simulation inputs involving Fe^{II} atoms, a spin-polarized DFT approach was used [40,41].

2.3. Processing of the Results

Each geometry-optimized configuration was processed using a series of home-made scripts to calculate the hereinafter listed characteristics.

The interaction energy E_{int} is defined as the difference between the potential energy of the entire system $E_{\text{MNT+HCB}}$ and the sum of the potential energies of its constituents, i.e., the potential energies of MNT, E_{MNT} (including the CCC), and the HCB molecule, E_{HCB}, and is calculated by employing the formula $E_{\text{int}} = E_{\text{MNT+HCB}} - [E_{\text{MNT}} + E_{\text{HCB}}]$.

To measure the change in the HCB molecular shape, the following quantity is calculated, referred to as the molecular shape distortion parameter δ, defined by the formula $\delta = \sum_i [\gamma_i - \gamma_{i,\text{eq}}]^2$, where γ_i and $\gamma_{i,\text{eq}}$ denote the values of i-th dihedral and equilibrium dihedral angle, respectively. The planar HCB molecule includes 64 dihedral angles in total, with the equilibrium values $\gamma_{i,\text{eq}}$ of either 0 or 180°.

The HCB-MNT plane-plane normal angle α is defined as the angle between two vectors normal to the planes of (i) MNT basal oxygens and (ii) HCB constituent atoms.

Further, a variety of Euclidean distances d_i between the HCB molecule (represented by its center of mass), the MNT surface (represented by a plane fitted to its basal oxygen atoms) and the nearest CCC is extracted from the atomic positions.

Finally, both the electron localization function (ELF) and the charge density (CHD) are directly obtained from single point energy calculations in VASP and the charge den-

sity difference is processed using the software VESTA [42] according to the formula $\rho(\boldsymbol{r}) = \rho_{\mathrm{MNT+HCB}}(\boldsymbol{r}) - [\rho_{\mathrm{MNT}}(\boldsymbol{r}) + \rho_{\mathrm{HCB}}(\boldsymbol{r})]$, where the symbol ρ stands for charge density at a spatial position $\boldsymbol{r}$.

3. Results and Discussion

As expected and previously shown in other works [11], after geometry optimization the compensating cations reside in the center of the ditrigonal cavity of the MNT's silicate sheet [11,20,43–45]. In general, the exact position of the compensating cations with respect to the z-axis (direction perpendicular to the layer surface) is determined by the size of the corresponding compensating cation in terms of its radius, its charge as well as the net charge of the surface and the thickness of the hydration shell [11,43–46]. Since the compensating cations here are the Ca^{2+} cations and, moreover, in this approximation are not hydrated, the distance between CCC and the basal oxygen atoms adopts values in a range between 0.3 and 1 Å as represented by the bottom line in Figure 2 ($d_{\mathrm{Ca^{2+}-O}}$ versus q). Very similar values were reported in previous works [11]. Figure 2 further demonstrates the importance of the MNT net surface charge. As the MNT net surface charge q increases, the CCC tends to be more attracted towards the surface resulting in the decrease of CCC-MNT distance by ≈60%.

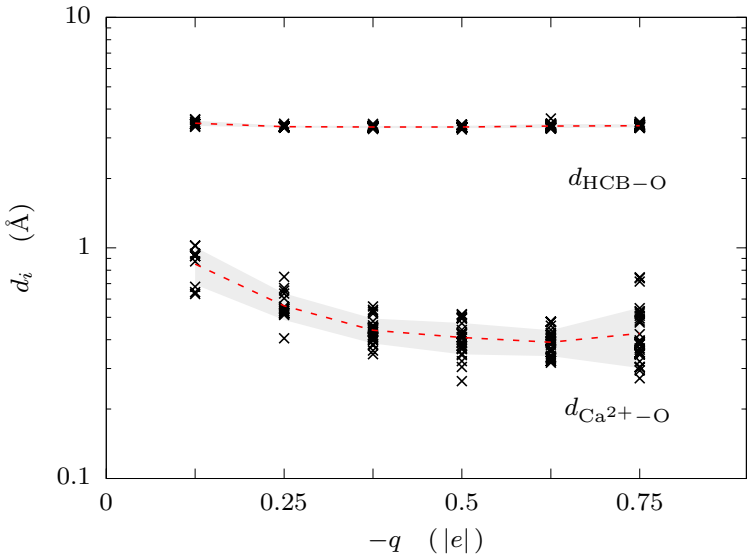

Figure 2. Euclidean distances d_i from the MNT basal oxygen atoms versus the MNT net surface charge q of the nearest CCC (with respect to the HCB molecule, $d_{\mathrm{Ca^{2+}-O}}$) and the center of mass of the HCB molecule ($d_{\mathrm{HCB-O}}$). The grey shaded areas and the dashed red lines correspond to the standard deviation of the collected data and the mean values, respectively.

The HCB molecule is attached to the nearest CCC by coordinating its aromatic ring to it and it has been speculated that this is mainly due to relatively strong cation-π interactions, typical for aromatic molecules, which are in contact with positively charged moieties [20]. By comparing both lines in Figure 2 ($d_{\mathrm{HCB-O}}$ and $d_{\mathrm{Ca^{2+}-O}}$ versus q), it becomes apparent that with the increasing MNT net surface charge, the distance between CCC and the MNT basal oxygen atoms decreases while the position of the HCB with respect to the MNT basal oxygen atoms remains almost unchanged. This can be explained by the above mentioned stronger attraction between CCC and MNT surface due to higher MNT net surface charge which very likely weakens the binding between the HCB and CCC but it does not affect the HCB position with respect to the MNT surface.

Figure 3 shows how both, the MNT net surface charge through the strength of the CCC-HCB interaction affects the planarity and rigidness of the HCB molecule. Keeping in mind that with increasing net layer charge the CCC-HCB interaction weakens and,

therefore, the overall shape distortion of the HCB molecule becomes smaller. On the other hand, lower values of the MNT net surface charge cause a significant shape distortion, as the distance between CCC and HCB becomes smaller (cf. Figure 2). It is important to note that the shape distortion involves only the orientation of the C-Cl bonds and cause greater polarization of the π molecular orbitals.

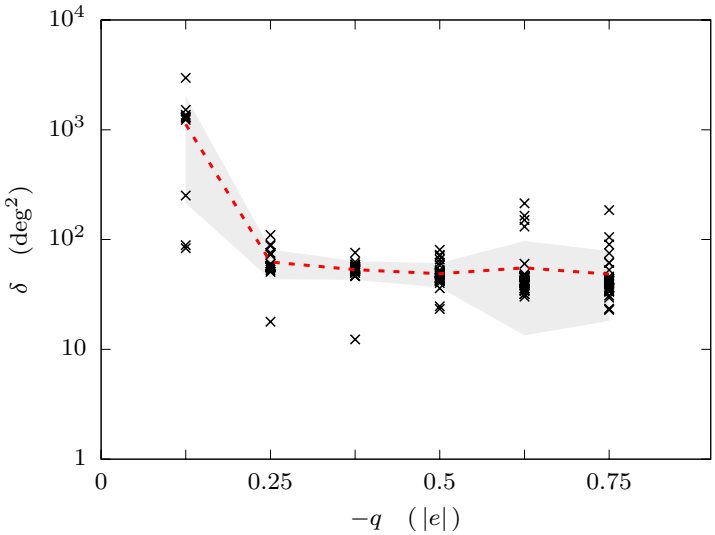

Figure 3. Molecular shape distortion parameter δ of HCB versus the MNT net surface charge q. The grey shaded area and the dashed red line correspond to the standard deviation of the collected data and the mean values, respectively.

As shown in Figure 4, the HCB-MNT plane-plane normal angles α extracted after geometry optimization procedure adopt values that never exceed 10°, suggesting that the overall orientation of the HCB molecular plane with respect to the MNT surface is parallel. Further, the relatively wide spread of the α values indicates that numerous similarly appearing minima exist on the potential energy surface and their complete exploration and categorization represents a challenging task [47].

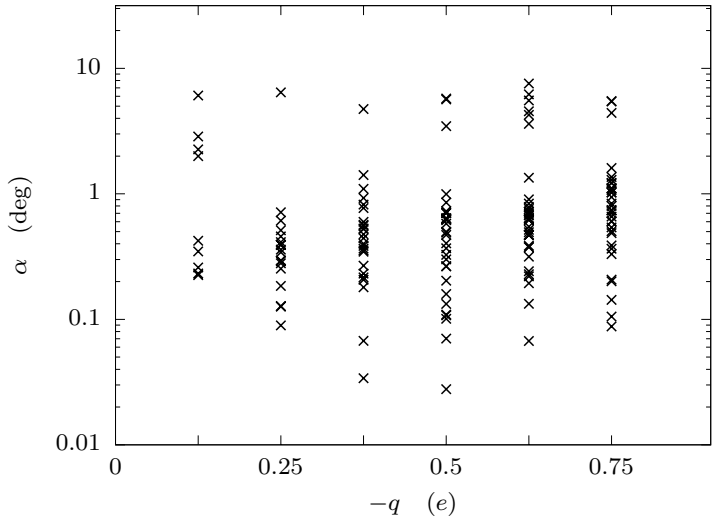

Figure 4. HCB-MNT plane-plane normal angles α versus the MNT net surface charge q.

Figure 5 shows the recorded distances between the nearest positioned CCC with respect to the HCB molecule, $d_{\mathrm{HCB-Ca^{2+}}}$. Two separate lines are clearly visible as a consequence of possibly two types of the molecular arrangement – first, in which the nearest

CCC lies close to the center of mass of the HCB molecule centered towards its hexagonal ring (bottom line) and second, in which the nearest CCC is positioned at least partly aside the HCB molecule (top line). Very similar separation of the recorded data is displayed in Figure 4.

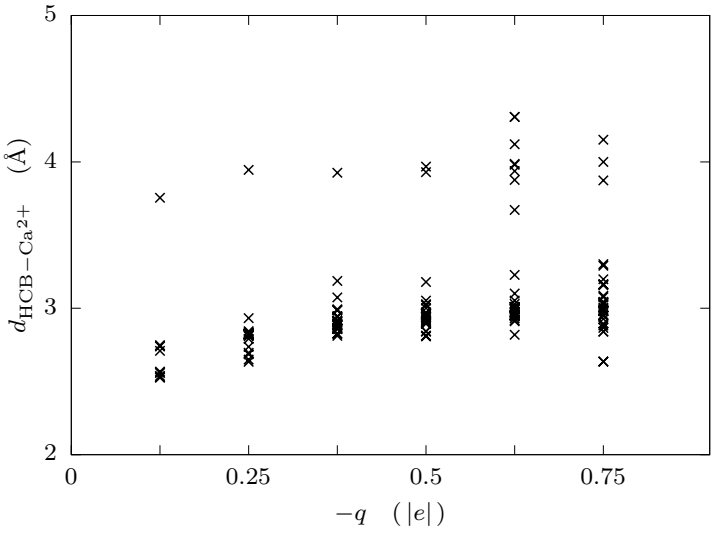

Figure 5. Euclidean distance between HCB and nearest CCC $d_{\mathrm{HCB-Ca^{2+}}}$ versus the MNT net surface charge q.

All these previous observations are summarized in the interaction energy dependence on the MNT net surface charge shown in Figure 6. The interaction energy E_{int} appears to be invariant to the MNT net layer charge q. The actual values are strongly scattered, and no clear trend can be spotted from the mean values estimates and their standard deviations that are used here to outline the data. As already mentioned, this might be a consequence of the existence of a large number of similarly appearing minima on the potential energy surface.

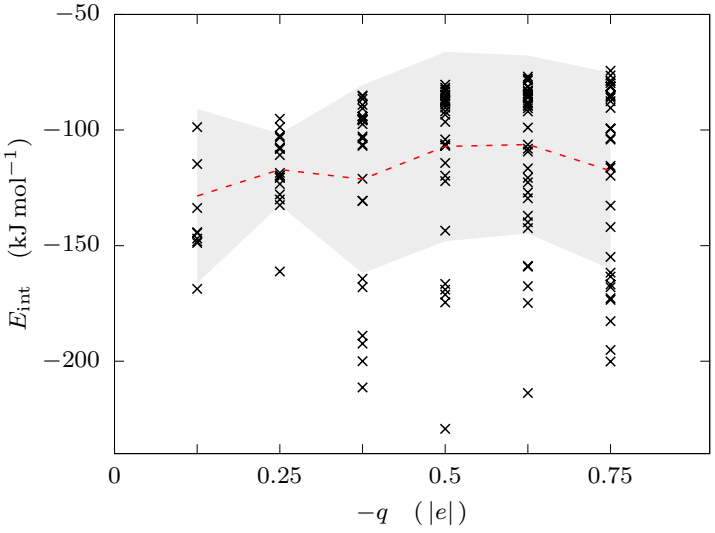

Figure 6. Interaction energies E_{int} versus MNT net surface charge q. The grey shaded area and the dashed red line correspond to the standard deviation of the collected data and the mean values, respectively.

As already mentioned, the scattered data in Figure 6 demonstrate that a large variety of relatively similar minima on the potential energy landscape exist. These are a consequence

of several factors, including the variations in the CCC positions with respect to the HCB molecule as well as the actual position of the nearest isomorphic substitutions. All these effects may play a significant role in the stability of the resulting HCB-MNT complex.

The electron localization function (ELF) displayed in Figure 7 demonstrates that the interactions between HCB and CCC as well as between CCC and MNT are a typical dispersion interactions [48]. Further, the electron clouds of the interacting bodies are at least partially polarized. This fact is more visible in Figure 8 in which the charge density difference is shown for two limiting cases. Lower values of the MNT net layer charge cause that electrons are depleted from (or accumulated to) greater volumes of the interacting bodies. This fact together with the greater change in the HCB molecular shape results (cf. Figure 3) in a greater polarization of the π molecular orbitals, again pointing towards the importance of cation-π interactions.

When it comes to the role of the MNT surface, the CHD plots in Figure 8 indicate that the interactions between the MNT with CCC and HCB involve exclusively the free electron pairs of the MNT's basal oxygen atoms.

It is important to note that the present results were obtained *in vacuo*, i.e., without the presence of solvent. The addition of solvent effects represents the next step in our research.

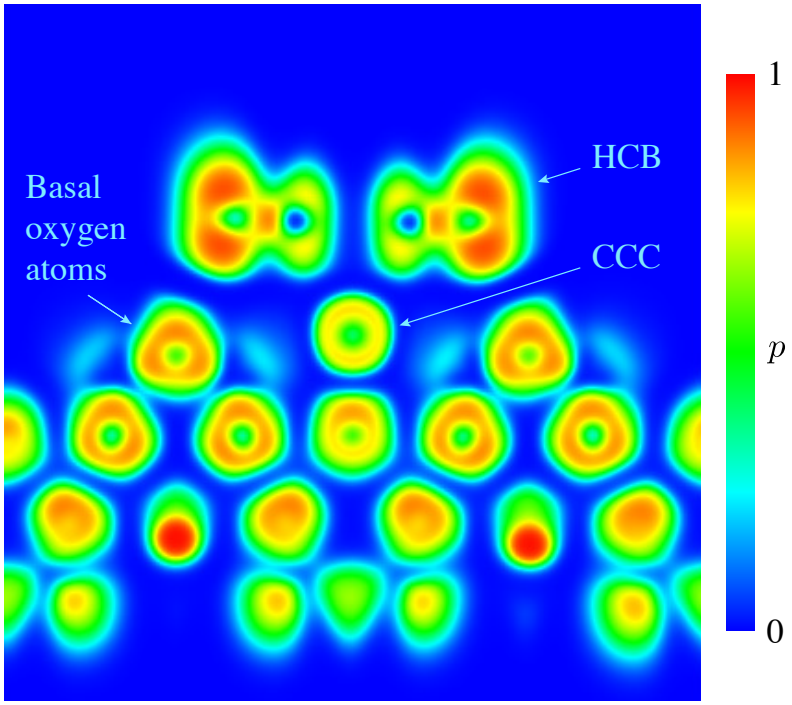

Figure 7. Electron localization function (ELF). The MNT-HCB complex is sliced through the center of the CCC. The color scheme represents the probability p of finding an electron at given spatial location. Snapshot corresponds to the MNT net surface charge of $-0.5\,|e|$.

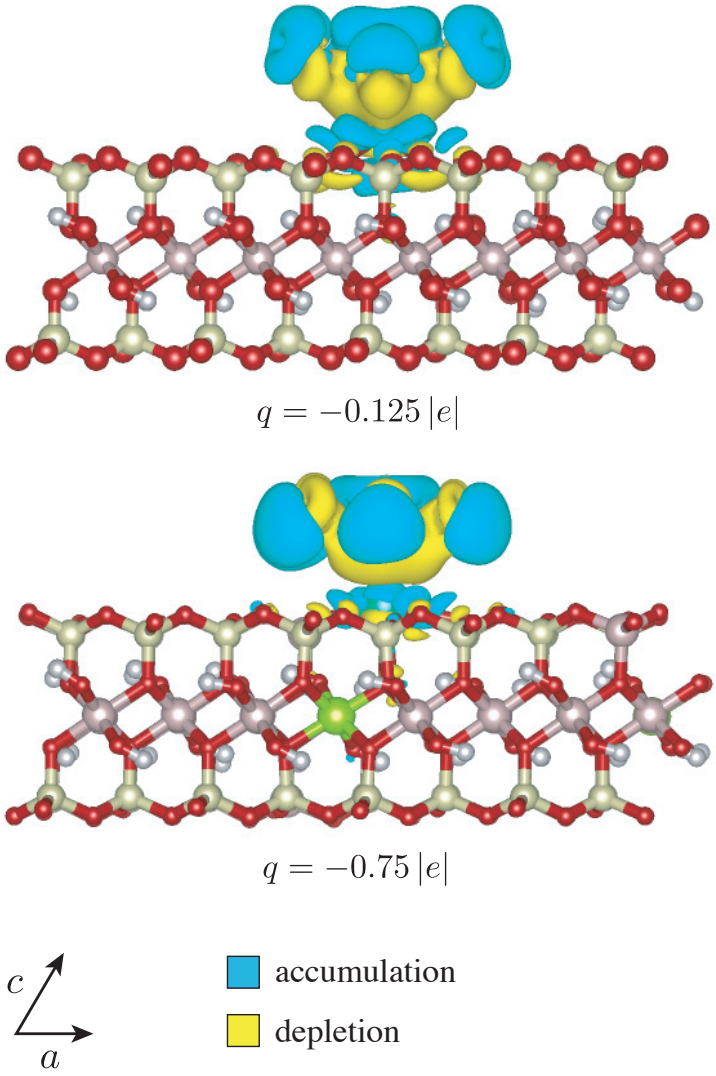

Figure 8. Charge density difference (CHD) for two limiting values of the MNT net surface layer charge q, i.e., -0.125 and $-0.75\,|e|$, respectively.

4. Conclusions

We investigated the adsorption of HCB to MNT surface by systematically varying the MNT net surface charge. It is evidenced that the adsorbed HCB molecule is always positioned at a constant distance from the MNT surface in a parallel orientation, regardless the actual value of the MNT net surface charge. On the other hand, the change in HCB molecular shape as well as the z-position of the CCC is found to depend on the MNT net surface charge. The calculated interaction energies demonstrate the existence of a large number of similarly appearing potential energy minima. It can be concluded that the dominant mechanism behind the HCB adsorption on MNT surface arises from cation-π interactions, therefore the type, valency, size and possible hydration of the CCC may have a strong impact on the stability of the HCB-MNT complexes.

Author Contributions: Conceptualization, P.G. and D.T.; methodology, P.G. and D.T.; software, P.G.; validation, P.G. and D.T.; formal analysis, P.G.; investigation, P.G.; resources, D.T.; data curation, M.H.G. and D.T.; writing—original draft preparation, P.G. and D.T.; writing—review and editing, P.G., L.B., M.H.G. and D.T.; visualization, P.G.; supervision, D.T. and M.H.G.; project administration, M.H.G.; funding acquisition, L.B. All authors have read and agreed to the published version of the manuscript.

Funding: This work has been supported by German Research Foundation (Deutsche Forschungsgemeinschaft, DFG), grant number 443637168, BO5388/1–1 and Austrian Science Fund (Fonds zur Förderung der Wissenschaftlichen Forschung, FWF), grant number I 4876–N in the bilateral project "Clay minerals as sorbents for hydrophobic organic chemicals—ClayHOC". The computational results presented have been achieved using the Vienna Scientific Cluster (VSC), project number 70544.

Institutional Review Board Statement: Not applicable.

Informed Consent Statement: Not applicable.

Data Availability Statement: Not applicable.

Conflicts of Interest: The authors declare no conflict of interest.

References

1. Barber, J.L.; Sweetman, A.J.; van Wijk, D.; Jones, K.C. Hexachlorobenzene in the global environment: Emissions, levels, distribution, trends and processes. *Sci. Total Environ.* **2005**, *349*, 1–44. [CrossRef]
2. Brahushi, F.; Kengara, F.O.; Song, Y.; Jiang, X.; Munch, J.C.; Wang, F. Fate Processes of Chlorobenzenes in Soil and Potential Remediation Strategies: A Review. *Pedosphere* **2017**, *27*, 407–420.
3. Haynes, W.M.; Lide, D.R. *Handbook of Chemistry and Physics*, 95th ed.; CRC Press; Taylor & Francis Group: Boca Raton, FL, USA, 2014.
4. Meijer, S.N.; Ockenden, W.A.; Sweetman, A.; Breivik, K.; Grimalt, J.O.; Jones, K.C. Global distribution and budget of PCBs and HCB in background surface soils: Implications for sources and environmental processes. *Environ. Sci. Technol.* **2003**, *37*, 667–672. [CrossRef] [PubMed]
5. Pan, B.; Ning, P.; Xing, B. Part IV—Sorption of hydrophobic organic contaminants. *Environ. Sci. Pollut. Res.* **2008**, *15*, 554–564. [CrossRef]
6. Karickhoff, S.W.; Brown, D.S.; Scott, T.A. Sorption of hydrophobic pollutants on natural sediments. *Water Res.* **1979**, *13*, 241–248. [CrossRef]
7. Chiou, C.T.; Malcolm, R.L.; Brinton, T.I.; Kile, D.E. Water solubility enhancement of some organic pollutants and pesticides by dissolved humic and fulvic acids. *Environ. Sci. Technol.* **1986**, *20*, 502–508. [CrossRef]
8. Ahmed, A.A.; Thiele-Bruhn, S.; Aziz, S.G.; Hilal, R.H.; Elroby, S.A.; Al-Youbi, A.O.; Leinweber, P.; Kühn, O. Interaction of polar and nonpolar organic pollutants with soil organic matter: Sorption experiments and molecular dynamics simulation. *Sci. Total Environ.* **2015**, *508*, 276–287. [CrossRef]
9. Böhm, L.; Düring, R.A.; Bruckert, H.J.; Schlechtriem, C. Can solid-phase microextraction replace solvent extraction for water analysis in fish bioconcentration studies with highly hydrophobic organic chemicals? *Environ. Toxicol. Chem.* **2017**, *36*, 2887–2894. [CrossRef]
10. Böhm, L.; Schlechtriem, C.; Düring, R.A. Sorption of highly hydrophobic organic chemicals to organic matter relevant for fish bioconcentration studies. *Environ. Sci. Technol.* **2016**, *50*, 8316–8323. [CrossRef]
11. Böhm, L.; Grančič, P.; Scholtzová, E.; Heyde, B.J.; Düring, R.A.; Siemens, J.; Gerzabek, M.H.; Tunega, D. Adsorption of the hydrophobic organic pollutant hexachlorobenzene to phyllosilicate minerals. *Environ. Sci. Pollut. Res. Int.* **2022**. [CrossRef]
12. Ferrage, E. Investigation of the Interlayer Organization of Water and Ions In Smectite from the Combined Use of Diffraction Experiments and Molecular Simulations. A Review of Methodology, Applications, And Perspectives. *Clays Clay Miner.* **2016**, *64*, 348–373. [CrossRef]
13. Anthony, J.W.; Bideaux, R.A.; Bladh, K.W.; Nichols, M.C. *Handbook of Mineralogy*; Mineralogical Society of America: Chantilly, VA, USA, 2003.
14. Bhattacharyya, K.G.; Gupta, S.S. Adsorption of a Few Heavy Metals on Natural and Modified Kaolinite and Montmorillonite: A Review. *Adv. Colloid Interface Sci.* **2008**, *140*, 114–131. [CrossRef] [PubMed]
15. Meier, L.P.; Nüesch, R. The Lower Cation Exchange Capacity Limit of Montmorillonite. *J. Colloid Interface Sci.* **1999**, *217*, 77–85. [CrossRef] [PubMed]
16. Pan, W.; Chang, J.; Liu, X.; Xue, Q.; Fu, J.; Zhang, A. Interfacial formation of environmentally persistent free radicals—A theoretical investigation on pentachlorophenol activation on montmorillonite in PM2.5. *Ecotoxicol. Environ. Saf.* **2019**, *169*, 623–630. [CrossRef]
17. Jia, H.; Zhao, S.; Shi, Y.; Zhu, L.; Wang, C.; Sharma, V.K. Transformation of Polycyclic Aromatic Hydrocarbons and Formation of Environmentally Persistent Free Radicals on Modified Montmorillonite: The Role of Surface Metal Ions and Polycyclic Aromatic Hydrocarbon Molecular Properties. *Environ. Sci. Technol.* **2018**, *52*, 5725–5733. [CrossRef]
18. Sainz-Díaz, C.I.; Francisco-Márquez, M.; Vivier-Bunge, A. Molecular structure and spectroscopic properties of polyaromatic heterocycles by first principle calculations: Spectroscopic shifts with the adsorption of thiophene on phyllosilicate surface. *Theor. Chem. Acc.* **2009**, *125*, 83–95. [CrossRef]
19. Hu, E.; Zhao, X.; Pan, S.; Ye, Z.; He, F. Sorption of nonionic aromatic organics to mineral micropores: Interactive effect of cation hydration and mineral charge density. *Environ. Sci. Technol.* **2019**, *53*, 3067–3077. [CrossRef]

20. Pašalić, H.; Aquino, A.J.A.; Tunega, D.; Haberhauer, G.; Gerzabek, M.H.; Lischka, H. Cation-π interactions in competition with cation microhydration: A theoretical study of alkali metal cation–pyrene complexes. *J. Mol. Model.* **2017**, *23*, 131. [CrossRef]
21. Qu, X.; Zhang, Y.; Li, H.; Zheng, S.; Zhu, D. Probing the Specific Sorption Sites on Montmorillonite Using Nitroaromatic Compounds and Hexafluorobenzene. *Environ. Sci. Technol.* **2011**, *45*, 2209–2216. [CrossRef]
22. Viani, A.; Gualtieri, A.F.; Artioli, G. The Nature of Dsorder in Montmorillonite by Simulation of X-ray Powder Patterns. *Am. Mineral.* **2002**, *87*, 966–975. [CrossRef]
23. Loewenstein, W. The Distribution of Aluminum in the Tetrahedra of Silicates and Aluminates. *Am. Mineral.* **1954**, *39*, 92–96.
24. Kresse, G.; Hafner, J. Ab initio molecular dynamics for liquid metals. *Phys. Rev. B* **1993**, *47*, 558–561. [CrossRef] [PubMed]
25. Kresse, G.; Hafner, J. Ab initio molecular-dynamics simulation of the liquid-metal-amorphous-semiconductor transition in germanium. *Phys. Rev. B* **1994**, *49*, 14251–14269. [CrossRef]
26. Kresse, G.; Furthmüller, J. Efficiency of ab-initio total energy calculations for metals and semiconductors using a plane-wave basis set. *Comput. Mater. Sci.* **1996**, *6*, 15–50. [CrossRef]
27. Kresse, G.; Furthmüller, J. Efficient iterative schemes for ab initio total-energy calculations using a plane-wave basis set. *Phys. Rev. B* **1996**, *54*, 11169. [CrossRef] [PubMed]
28. Bučko, T.; Hafner, J.; Ángyán, J.G. Geometry optimization of periodic systems using internal coordinates. *J. Chem. Phys.* **2005**, *122*, 124508. [CrossRef]
29. Perdew, J.P.; Chevary, J.A.; Vosko, S.H.; Jackson, K.A.; Pederson, M.R.; Singh, D.J.; Fiolhais, C. Atoms, molecules, solids, and surfaces: Applications of the generalized gradient approximation for exchange and correlation. *Phys. Rev. B* **1992**, *46*, 6671–6687. [CrossRef]
30. Perdew, J.P.; Burke, K.; Ernzerhof, M. Generalized gradient approximation made simple. *Phys. Rev. Lett.* **1996**, *77*, 3865–3868. [CrossRef]
31. Bučko, T.; Lebègue, S.; Hafner, J.; Ángyán, J.G. Tkatchenko-Scheffler van der Waals correction method with and without self-consistent screening applied to solids. *Phys. Rev. B* **2013**, *87*, 064110. [CrossRef]
32. Tunega, D.; Bučko, T.; Zaoui, A. Assessment of ten DFT methods in predicting structures of sheet silicates: Importance of dispersion corrections. *J. Chem. Phys.* **2012**, *137*, 114105. [CrossRef]
33. Tunega, D.; Zaoui, A. Adsorption of polycyclic aromatic hydrocarbons on FeOOH polymorphs: A theoretical study. *Surf. Sci.* **2021**, *706*, 121795. [CrossRef]
34. Grimme, S.; Antony, J.; Ehrlich, S.; Krieg, H. A consistent and accurate ab initio parametrization of density functional dispersion correction (DFT-D) for the 94 elements H-Pu. *J. Chem. Phys.* **2010**, *132*, 154104. [CrossRef] [PubMed]
35. Becke, A.D.; Johnson, E.R. A density-functional model of the dispersion interaction. *J. Chem. Phys.* **2005**, *123*, 154101. [CrossRef] [PubMed]
36. Johnson, E.R.; Becke, A.D. A post-Hartree–Fock model of intermolecular interactions. *J. Chem. Phys.* **2005**, *123*, 024101. [CrossRef]
37. Johnson, E.R.; Becke, A.D. A post-Hartree-Fock model of intermolecular interactions: Inclusion of higher-order corrections. *J. Chem. Phys.* **2006**, *124*, 174104. [CrossRef]
38. Blochl, P.E. Projector augmented-wave method. *Phys. Rev. B* **1994**, *50*, 17953–17979. [CrossRef]
39. Kresse, G.; Joubert, D. From ultrasoft pseudopotentials to the projector augmented-wave method. *Phys. Rev. B* **1999**, *59*, 1758–1775. [CrossRef]
40. Hohenberg, P.; Kohn, W. Inhomogeneous electron gas. *Phys. Rev.* **1964**, *136*, B864–B871. [CrossRef]
41. Kohn, W.; Sham, L.J. Self-Consistent Equations Including Exchange and Correlation Effects. *Phys. Rev.* **1965**, *140*, A1133–A1138. [CrossRef]
42. Momma, K.; Izumi, F. VESTA 3 for three-dimensional visualization of crystal, volumetric and morphology data. *J. Appl. Crystallogr.* **2011**, *44*, 1272–1276. [CrossRef]
43. Chatterjee, A.; Iwasaki, T.; Ebina, T.; Miyamoto, A. A DFT study on clay–cation–water interaction in montmorillonite and beidellite. *Comput. Mater. Sci.* **1999**, *14*, 119–124. [CrossRef]
44. Chatterjee, A.; Iwasaki, T.; Ebina, T. A Novel Method to Correlate Layer Charge and the Catalytic Activity of 2:1 Dioctahedral Smectite Clays in Terms of Binding the Interlayer Cation Surrounded by Monohydrate. *J. Phys. Chem. A* **2000**, *104*, 8216–8223. [CrossRef]
45. Li, H.; Kang, T.; Zhang, B.; Zhang, J.; Ren, J. Influence of interlayer cations on structural properties of montmorillonites: A dispersion-corrected density functional theory study. *Comput. Mater. Sci.* **2016**, *117*, 33–39. [CrossRef]
46. Seppälä, A.; Puhakka, E.; Olin, M. Effect of layer charge on the crystalline swelling of Na^+, K^+ and Ca^{2+} montmorillonites: DFT and molecular dynamics studies. *Clay Miner.* **2016**, *51*, 197–211. [CrossRef]
47. Bowal, K.; Grančič, P.; Martin, J.W.; Kraft, M. Sphere Encapsulated Monte Carlo: Obtaining Minimum Energy Configurations of Large Aromatic Systems. *J. Phys. Chem. A* **2019**, *123*, 7303–7313. [CrossRef]
48. Koumpouras, K.; Larsson, J.A. Distinguishing between chemical bonding and physical binding using electron localization function (ELF). *J. Phys. Condens. Matter* **2020**, *32*, 315502. [CrossRef]